Key Engineering Materials
ISSN: 1662-9795, Vol. 1047, pp 205-212

Submitted: 2026-01-19
Revised: 2026-02-13
Accepted: 2026-02-14
Online: 2026-04-13

Thermal Measurement During High-Velocity Oxy-Fuel Coating Process for Single and Multiple Pass Rotational Spraying

Diyoke George[1,a*], Yang Yitong[2,b], Schindelbacher Christoph[3,c], Sperling Sebastian[3,d], Angerler Jürgen[3,e] and Härtel Sebastian[1,f]

[1]Chair of Hybrid Manufacturing, Brandenburg University of Technology, Cottbus, Germany

[2]Chair of Metallurgy and Material Engineering, Brandenburg University of Technology, Cottbus, Germany

[3]Voith Austria GmbH, VPRW Betriebsstätte, Wimpassing, Austria

[a*]diyoke@b-tu.de, [b]yang@b-tu.de, [c]christoph.schindelbacher@voith.com, [d]sebastian.sperling@voith.com, [e]juergen.angerler@voith.com, [f]sebastian.Haertel@b-tu.de

Keywords: high-velocity oxy-fuel, thermal measurements, heat source, coating process.

Abstract. High-velocity oxy-fuel spraying is a widely used thermal spray technology for producing dense and wear-resistant coatings. The thermal input during spraying strongly influences coating microstructure, residual stress state, and substrate integrity. In this work, in situ thermal measurements were performed on S235 substrates during High-velocity oxy-fuel deposition of 316L coatings. Two spraying strategies were compared: (i) single-pass rotation and (ii) multi-pass rotation. Thermocouples embedded at 1.8mm depth captured transient temperature responses, revealing significant thermal cycling effects. Single-pass operations produced no significant heating–cooling cycles, while multi-pass strategies led to thermal accumulation and overlapping cycles. The results provide reference data for the calibration of finite element heat source models and support the development of process–structure–property relationships in High-velocity oxy-fuel coatings.

Introduction

Austenitic stainless steel, particularly 316L, is well known for its excellent corrosion resistance and mechanical reliability, which makes it an attractive candidate for use as a protective coating material [1].

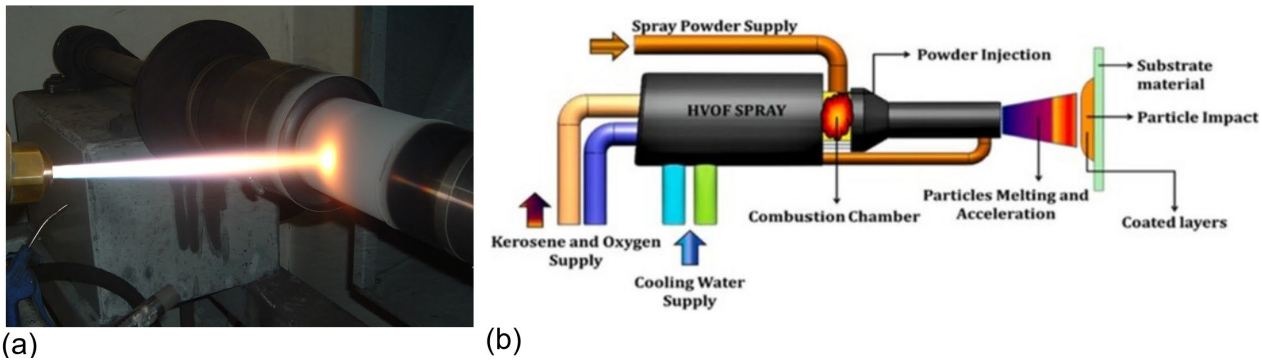

Fig. 1. Process set up (a) HVOF spraying setup showing the combustion-driven jet impinging on a rotating cylindrical substrate; (b) schematic of the HVOF gun, illustrating kerosene/oxygen combustion, particle acceleration, and deposition on the substrate [2].

High-velocity oxy-fuel (HVOF) spraying offers an effective deposition route by accelerating semi-molten particles toward the substrate, promoting dense, well-bonded coatings with reduced porosity and limited oxide formation compared to atmospheric plasma spraying (APS). As illustrated in Fig. 1(a), HVOF produces a distinct thermal footprint, while Fig. 1(b) shows how kerosene–oxygen combustion drives particles toward the substrate at high velocity. Upon impact, these particles plastically deform into splats, consolidating the coating and enhancing densification. Although HVOF substantially improves coating density and minimizes oxidation, thin oxide films, localized

porosity, and subtle compositional shifts may still form during deposition and can influence the passive-film stability of 316L stainless steel in aggressive environments [3]. Understanding how these deposition dynamics affect microstructure, residual stresses, and coating performance requires investigation at both the splat and coating process scales.

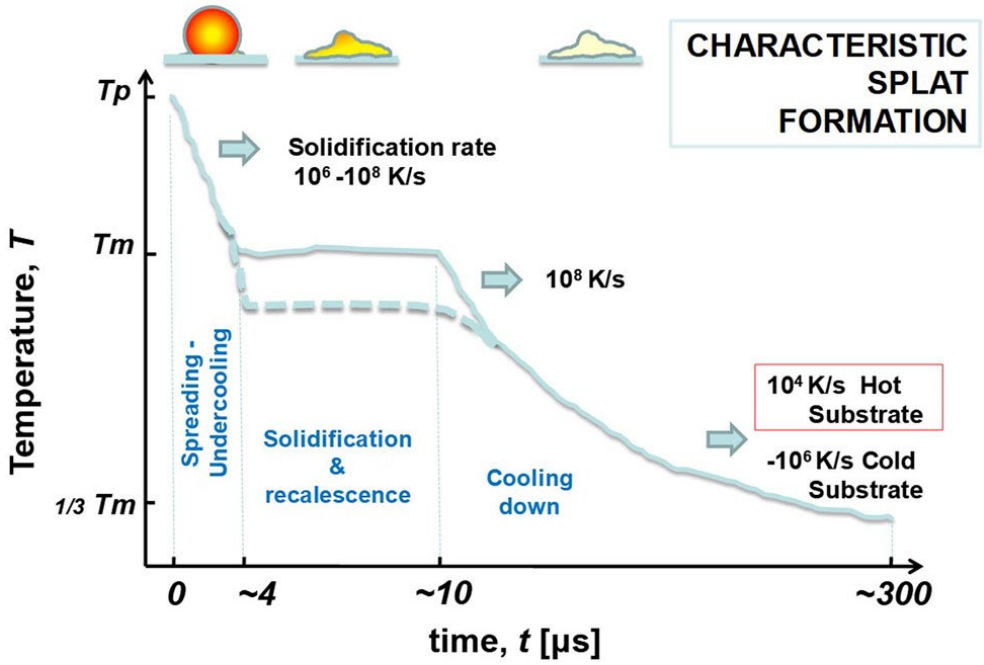

Fig. 2. Schematic illustration of the splat formation during coating with respect to temperature and time history. This captures the: process of particle spreading, solidification, recalescence, and final cooling. Undercooling is represented in dashed line [4].

During thermal spraying such as HVOF, coating build-up occurs through the successive splat formation which involves: (1) impact and spreading (2) solidification (with release of latent heat) and (3) cooling of individual semi-molten particles [4, 5, 6]. As shown schematically in Fig. 2, splat formation is an ultrafast, highly transient process characterized by extreme cooling and solidification rates [4]. Upon impact with the substrate, a molten particle spreads radially within a few microseconds, during which rapid heat extraction leads to significant undercooling below the equilibrium melting temperature. Solidification initiates only after the completion of spreading and is accompanied by recalescence due to latent heat release following droplet impact and rapid heat extraction to the substrate [7, 8]. Because this phase transformation occurs under strong thermal gradients with constrained shrinkage against the substrate, and transformation strains are generated and locked into the splat. Subsequent cooling of the fully solidified splat toward the substrate temperature further contributes to stress development through thermal mismatch effects [9]. These coupled thermo-mechanical phenomena at the splat scale are decisive in residual stress evolution in thermal spray coatings.

At the coating–substrate scale, the fundamental mechanisms of splat formation and adherence are strongly influenced by the cumulative residual stresses generated during successive particle impacts [10]. The thermal and mechanical response of an HVOF coating is ultimately controlled by the combined thermal history imposed by particle deposition and torch motion. Capturing this highly transient heat transfer exceeds the resolution of experimental techniques and requires finite element modeling. Moving heat source models, similar to those used in weld simulations, allow simulation of local transient heating, cooling rates, and thermal gradients induced by the moving energy source [11, 12, 13]. The predictive capability of such models depends critically on accurate heat source descriptions, realistic thermal boundary conditions, and proper accounting of spatial and temporal variations in heat input due to spray kinematics, pass strategy, and coating build-up. This approach enables reliable correlations between process parameters, resulting microstructure, and coating properties.

In this study, in situ thermal measurements were conducted during HVOF deposition of 316L stainless steel on S235 structural steel, comparing single-pass and multi-pass rotational spraying. The thermal histories across the spray footprint were correlated with coating thickness, microstructure evolution, and hardness distribution. A finite element–based heat source model, incorporating appropriate boundary conditions, was developed to capture the thermal behavior of the process. This analysis provides new insights into the process–microstructure–property relationships of HVOF-sprayed 316L coatings.

Material and Methods

S235 structural-steel plate in Fig. 1(a) of dimension **L**100x**W**100x**H**10mm^3 is used as substrates and roughened through sand blasting to Rz~40 µm. The experimental arrangement for mounting and processing the samples is illustrated in **Fig. 2(b)**. The coating material is a gas-atomized 316L stainless-steel powder with a particle-size distribution of nominal (-53µm/+20µm).

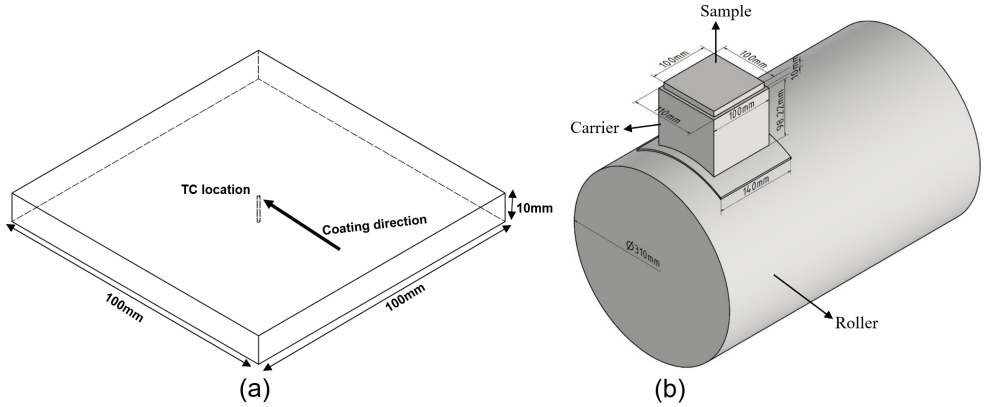

Fig. 3. Experimental set up of the process for thermal measurement; (a) the location of the thermocouple (TC) at the centre of the substrate and approximately 1.8mm away from the substrate surface; and (b) the sample mounted on rotating roller with a carrier a carrier which protects the thermal measurement device.

Coatings were deposited using a HVOF torch mounted on a programmable robotic system. As illustrated in Fig. 1(a), the substrates were mounted on a carrier and fixed onto a rotating cylindrical roller of 310 mm diameter, rotating at 100 rpm. Two spraying strategies were evaluated: (1) Single-pass rotation, in which the cylinder completed one full rotation while the torch kept fixed at a specific distance; and (2) Multi-pass rotation, consisting of 20 and 40 consecutive passes. Other process parameters used for the experiment are detailed in Table 1.

Table 1. Parameters for high velocity oxy fuel process.

Powder particles	Kerosene flow rate /(Lh^{-1})	Oxygen flow rate/(Lmin^{-1})	Nitrogen flow rate/ (Lmin^{-1})	Rotational speed of the roller/(rpm)	Maximum thickness/(µm)	Spray distance/mm
316L	~15-20	~850-900	~1.5	100	400	~200-300

The thermocouple location is depicted in Fig. 2(a). Type-K thermocouples were embedded 1.8 mm below the substrate surface at the spray-center position. Temperature data were sampled at 10 Hz using a data logger, and thermal histories are recorded for both single- and multi-pass conditions. Cross-sections were prepared using standard metallographic procedures. Microstructural characterization is carried out using a Keyence VHX-7000 digital microscope. Electron backscatter diffraction (EBSD) measurements were performed on mechanically polished cross-sections using a step size of 0.02µm. Hardness measurements is performed on polished sample surfaces using a ZwickRoell Durascan 70 G5 (EMCO-TEST) equipped with a Vickers indenter, applying a 200 g load with a spacing of 1.0 mm between indentations.

Process Model

To infer the temperature evolution within the coating layer, a 3D finite element model incorporating a moving heat source is developed using Simufact numerical tool. As a first approximation, the heat source was represented as a cylindrical volumetric heat source with a radius of 50 mm, introducing thermal energy exclusively into the coating layer. The substrate heating occurred solely through heat transfer from the hot coating layer to the colder substrate. The basic model setup is illustrated in Fig. 4, where a finer mesh is used in the coating and adjacent substrate to capture the thermal history, and a coarser mesh is applied to the remaining substrate.

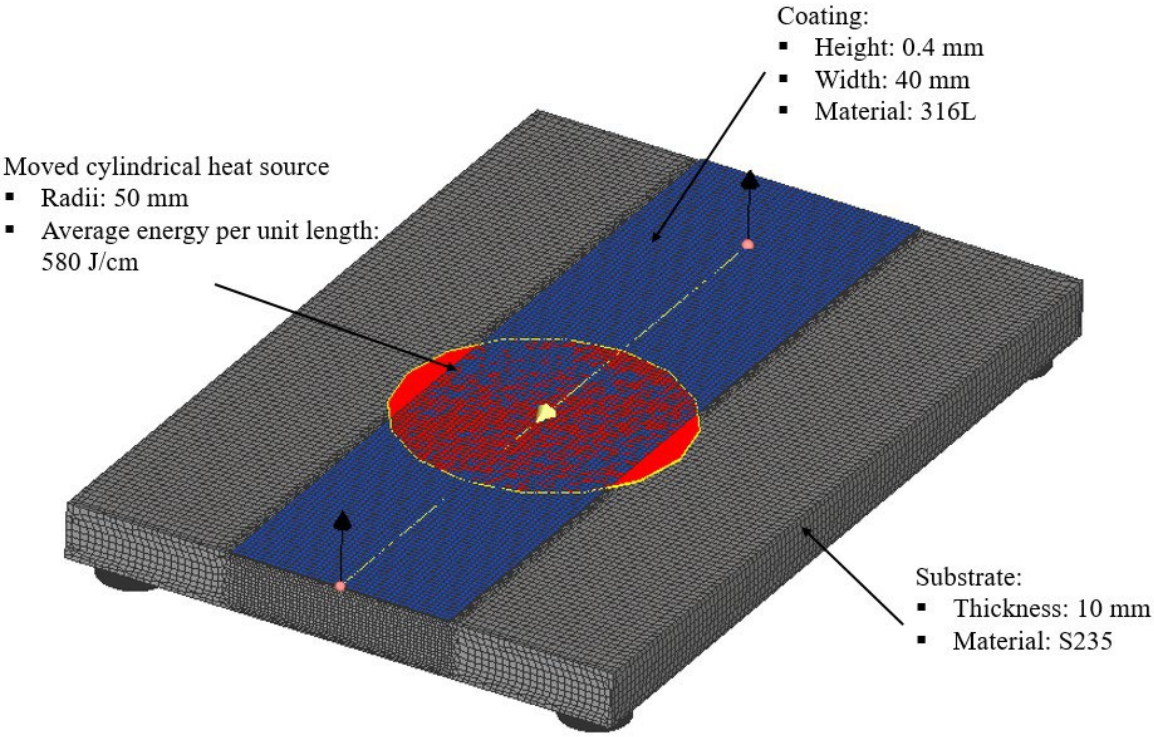

Fig. 4. Schematic illustration of the process set showing moving cylindrical heat source.

The cylindrical heat source represents a spatially averaged approximation of the effective thermal footprint of the HVOF jet.

Table 2. Simulation Input Parameters.

Category	Parameter	Symbol	Value
Geometry	Substrate dimensions	–	100 × 100 × 10 mm³
Geometry	Coating dimensions	–	100 × 40 × 0.4 mm³
Process control	Velocity	v	1620 mm/s
Heat source	radii	r	50 mm
Heat source	depth	d	0.15mm
Heat source	Average energy	E	580 J/cm
Boundary condition	Convection coefficient to air	h	300 $W \cdot m^{-2} \cdot K^{-1}$

The heat-source power was determined using an inverse calibration approach. Specifically, the heat input was iteratively adjusted until the calculated temperature at the measurement location (1.8 mm below the substrate surface) matched the experimentally measured temperature. This procedure resulted in an average energy input per unit length of 580 J/cm, which was subsequently used for all simulations. Other simulation input parameters are listed in Table 2.

Results and Discussion

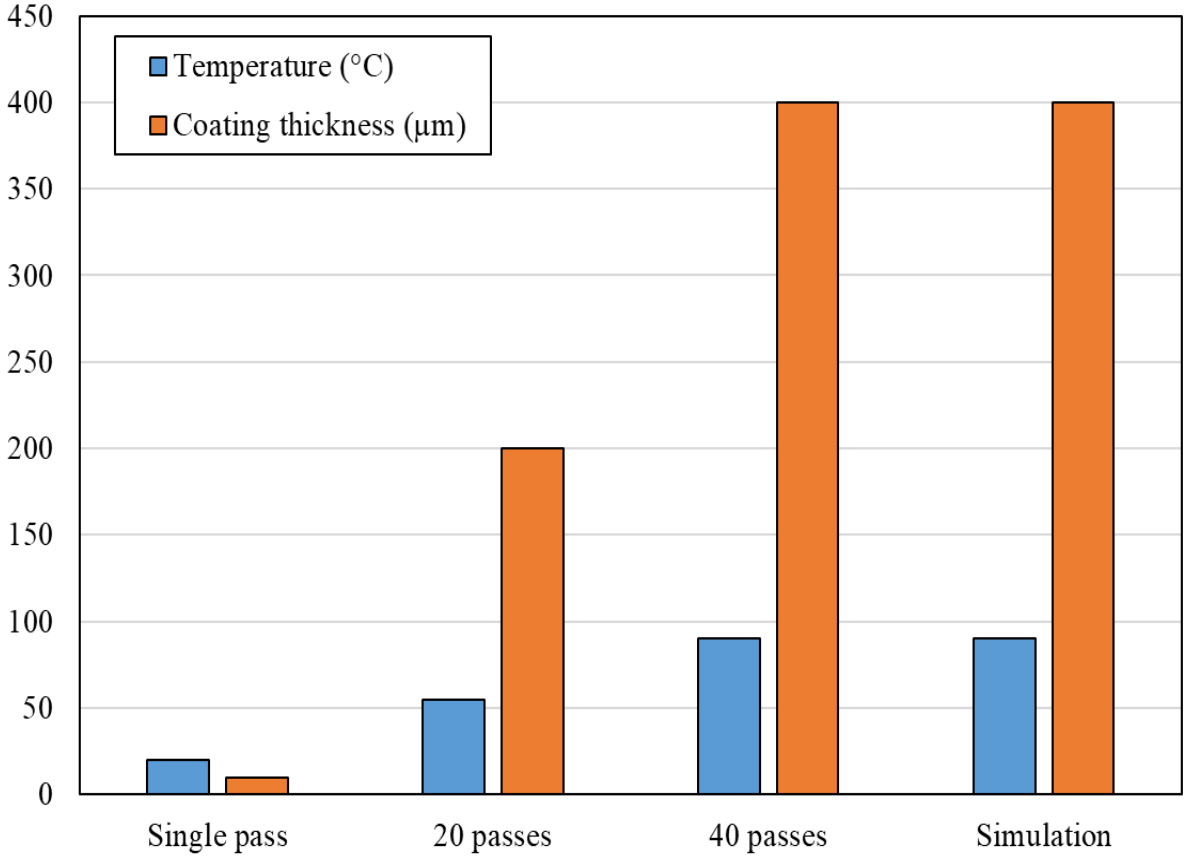

Fig. 5. Substrate maximum temperature and coating thickness of single-pass, multi-pass and validation of multi-pass during HVOF spraying.

Fig. 5 illustrates the maximum substrate temperature and corresponding coating thickness achieved for single- and multi-pass HVOF spraying as well as numerical validation. For the single-pass deposition, the temperature in the substrate remains low, with a corresponding low thickness achieved. In contrast, multi-pass rotation results in a significant increase in maximum substrate temperature, reaching approximately 50–55 °C after 20 passes and further rising to about 90 °C for 40 passes. The trend indicates accumulation of heat in successive passes during coating. The results also show good agreement with simulated temperature and thickness predictions for 40 passes. Thermal accumulation during multi-pass rotation may play a key role in determining the final microstructural and mechanical properties of the deposited layer, which will be discussed next.

The thermal and geometric evolution of the HVOF coating during the two-stage deposition process offers critical insight into how particle flux distribution, heat accumulation, and impact dynamics govern the resulting microstructure. In Fig. 6(a) no significant deposit is observed after single pass spraying which align with the absence of thermal cycle recorded and room temperature reported in Fig. 5. In contrast, as shown in Fig. 6(b), repeated spraying produces a pronounced convex profile at the center of the spray track. After approximately 20–40 passes, the coating reaches a maximum thickness of about 400 µm at the center, while the edges accumulate substantially less material due to the divergent expansion of the particle jet as it exits the nozzle.

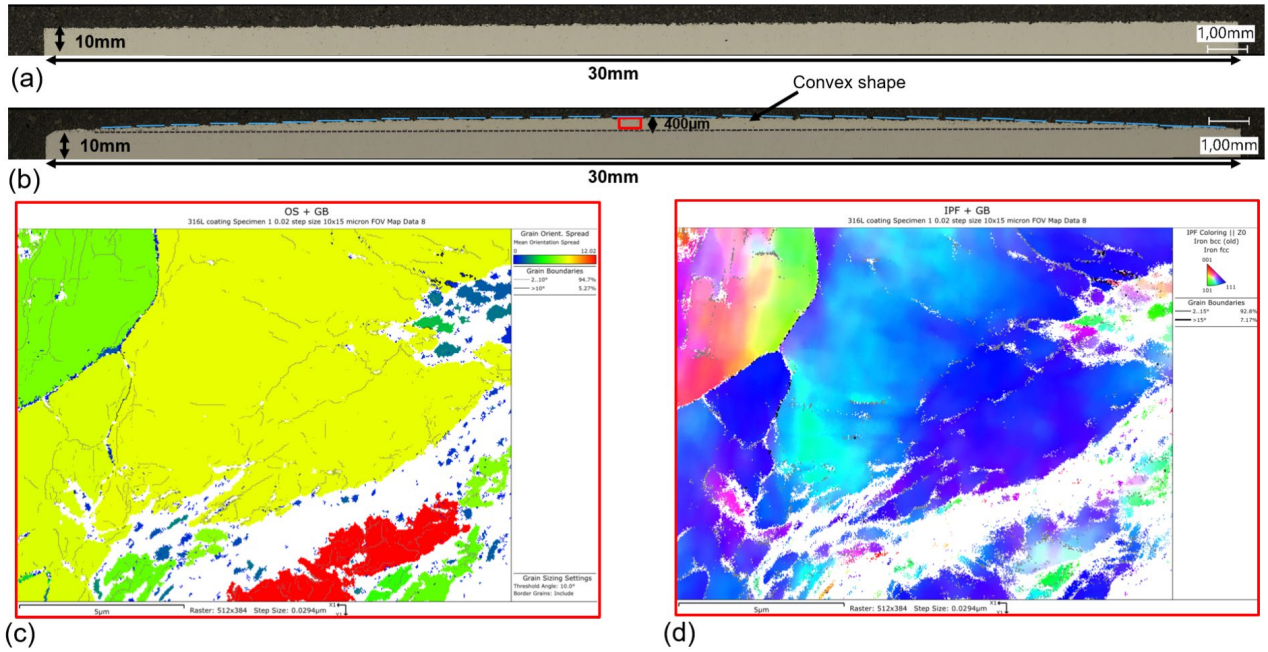

Fig. 6. Coating thickness profiles and representative cross section micrographs and grain properties. (a) Coating thickness profile after single pass; (b) coating thickness profile after 20–40 passes showing the pronounced convex geometry and maximum centre thickness of 400 µm; (c) GOS map, and (d) IPF map (both c and d are magnifications from the center region in red box in b).

Fig. 6(c) shows the grain orientation spread (GOS), with most grains exhibiting values above 10°, which is significantly higher than the values typically associated with dynamic recrystallization (<3°). Furthermore, Fig. 6(d) shows the distribution of grain boundary angles, with a predominance of low-angle boundaries 92.8% of the boundaries have angles below 15° which contrasts with the microstructural indication of continuous dynamic recrystallization, generally characterized by the progressive transformation of low-angle to high-angle boundaries. Together, these observations indicate that the microstructure reflects an absence of dynamic recrystallization rather than its occurrence. At the macroscopic scale, the coating geometry formed during multi-pass rotation reflects the spatial distribution of particle and heat flux inherent to the HVOF jet.

The convex coating morphology observed for the multi-pass is consistent with the Gaussian-type particle flux distribution characteristic of HVOF jets. The observed deposition profile aligns with the Gaussian heat source model widely used in literature for simulation. The fundamental expression that relates heat flux with the coating width reads [9]:

$$q(r) = q_0 \exp\left(-\frac{r^2}{2\sigma^2}\right) \quad (1)$$

where q_0 is the peak heat flux at the centerline and σ defines the coating width. In the present study, the convective heating pattern and coating build-up strongly mirror this Gaussian behavior: the maximum temperature rise (~90 °C) and the thickest coating (~400 µm) occur at the same center region where particle flux and heat flux are theoretically highest. Toward the edges (~10 mm away from the center), reduced heat input predicted by the Gaussian curve is consistent with the reduced particle flattening and lower coating thickness observed. Fig. 7 shows the temperature field under quasi-steady-state process conditions; the numerically determined maximum temperature reached in the layer is approximately 850 °C.

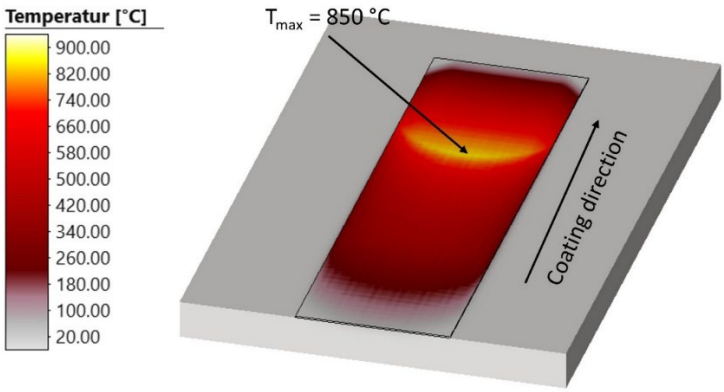

Fig. 7. Simulated spatial temperature distribution of the coated layer.

The microstructural, geometric, and thermal variations are reflected in the spatial distribution of hardness across the coating.

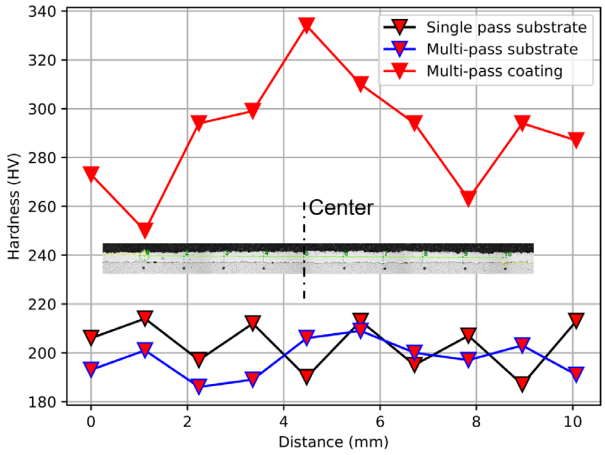

Fig. 8. Hardness distribution across the coating and substrate width.

Hardness profiles measured across the 10 mm-wide coated centreline (Fig. 8) further support the microstructural trends observed in Fig. 6(b). The coating exhibits substantially higher hardness values of approximately 250–340 HV at the centre. The highest hardness occurs at the region of maximum coating thickness and particle flux, consistent with intensified impact energy and enhanced local densification. The S235 substrate maintains a hardness of 185–215 HV for both single-pass and multi-pass conditions, reflecting its limited thermal exposure; even after 20–40 passes. Overall, the combined effects of progressive heat accumulation and plastic deformation during successive passes explain the localized microstructural changes in the thickest region, corresponding to the observed increase in hardness.

Conclusion

The single- and multi-pass thermal evolution exhibits a systematic increase with coating thickness. In multi-pass deposition, the coating thickness is highest at the center and decreases toward the periphery, resulting in a convex, Gaussian-like profile. This geometry, together with the localized hardness peak at the track center, is associated with regions of higher particle flux and cumulative thermal input, while no evidence of dynamic recrystallization was observed. Overall, these results establish a clear quantitative and qualitative relationship between process parameters, microstructure, and mechanical response in the HVOF process. The FE heat source model, calibrated using in situ temperature measurements, successfully reproduces the experimentally observed thermal accumulation during multi-pass rotation and supports interpretation of the measured trends. Future work will include repeated experimental trials to quantify statistical variability and further strengthen the reliability of the derived thermal trends and model calibration.

Funding

The authors acknowledge financial support from the Deutsche Forschungsgemeinschaft (DFG) under Project HeatCoatRoll, Grant No. 539450784.

References

[1] Y.B. Lei, Z.B. Wang, B. Zhang, Z.P. Luo, J. Lu, K. Lu, Enhanced mechanical properties and corrosion resistance of 316L stainless steel by pre-forming a gradient nanostructured surface layer and annealing, Acta Mater. 208 (2021) 116773. https://doi.org/10.1016/j.actamat.2021.116773.

[2] S. Kumar, D.C. Prasad, H. Hanumanthappa, Role of Thermal Spray Coatings on Erosion, Corrosion, and Oxidation in Various Applications: A Review, J. Bio-Tribo-Corros. 10 (2024) 22. https://doi.org/10.1007/s40735-024-00822-8.

[3] S. Kuroda, T. Fukushima, M. Sasaki, T. Kodama, Microstructure and Corrosion Resistance of HVOF Sprayed 316L Stainless Steel and Hastelloy C Coatings, Mater. Trans. 43 (2002) 3177–3183. https://doi.org/10.2320/matertrans.43.3177.

[4] A. Valarezo, K. Shinoda, S. Sampath, Effect of deposition rate and deposition temperature on residual stress of HVOF-sprayed coatings, *J. Therm. Spray Technol.* **29** (6) (2020) 1322–1338. https://doi.org/10.1007/s11666-020-01073-y.

[5] S. Sampath, X. Jiang, J. Matejicek, A. Leger, A. Vardelle, Substrate temperature effects on splat formation, microstructure development and properties of plasma sprayed coatings Part I: Case study for partially stabilized zirconia, *Mater. Sci. Eng. A* **272** (1) (1999) 181–188.

[6] K. Shinoda, Y. Kojima, T. Yoshida, In situ measurement system for deformation and solidification phenomena of yttria-stabilized zirconia droplets impinging on quartz glass substrate under plasma-spraying conditions, *J. Therm. Spray Technol.* **46** (2005) 98.

[7] K.-C. Chang, C.-M. Chen, Revisiting heat transfer analysis for rapid solidification of metal droplets, *Int. J. Heat Mass Transf.* **44** (8) (2001) 1573–1583. https://doi.org/10.1016/S0017-9310(00)00193-9.

[8] S. Chandra, P. Fauchais, Formation of solid splats during thermal spray deposition, *J. Therm. Spray Technol.* **18** (2009) 148–180. https://doi.org/10.1007/s11666-009-9294-5.

[9] A. Fardan, R. Ahmed, Modeling the evolution of residual stresses in thermally sprayed YSZ coating on stainless steel substrate, *J. Therm. Spray Technol.* **28** (4) (2019) 717–736. https://doi.org/10.1007/s11666-019-00856-2.

[10] P. Bansal, P.H. Shipway, S.B. Leen, Residual stresses in high-velocity oxy-fuel thermally sprayed coatings – Modelling the effect of particle velocity and temperature during the spraying process, *Acta Mater.* **55** (15) (2007) 5089–5101. https://doi.org/10.1016/j.actamat.2007.05.031

[11] Goldak, J., Chakravarti, A., & Bibby, M. (1984). *A new finite element model for welding heat sources*. Metallurgical Transactions B, 15(2), 299–305.

[12] Zhang, X., Li, S., & Kovacevic, R. (2005). *Finite element modeling of heat transfer in laser-based surface engineering processes*. International Journal of Machine Tools and Manufacture, 45(10), 1135–1145.

[13] S. Haertel, A. Schmidt, J. Szyndler, Determination of welding heat source parameters for FEM simulation based on temperature history and real bead shape, in: *Proceedings*, (2023) 159–168. https://doi.org/10.21741/9781644902479-18.